
ENTROPY-REGULARIZED GRADIENT ESTIMATORS FOR APPROXIMATE BAYESIAN INFERENCE

Jasmeet Kaur

Department of Computer Science
University of Texas, Austin

ABSTRACT

Effective uncertainty quantification is important for training modern predictive models with limited data, enhancing both accuracy and robustness. While Bayesian methods are effective for this purpose, they can be challenging to scale. When employing approximate Bayesian inference, ensuring the quality of samples from the posterior distribution in a computationally efficient manner is essential. This paper addresses the estimation of the Bayesian posterior to generate diverse samples by approximating the gradient flow of the Kullback-Leibler (KL) divergence and the cross entropy of the target approximation under the metric induced by the Stein Operator. It presents empirical evaluations on classification tasks to assess the method’s performance and discuss its effectiveness for Model-Based Reinforcement Learning that uses uncertainty-aware network dynamics models.

1 Introduction

Deep Learning models often result in overconfident and miscalibrated predictions without uncertainty quantification. It becomes more important when limited data is available, the quality of data available is poor, or one needs to consider making out-of-distribution predictions. These cases find their use in real-world situations that require safe decision-making. Measuring uncertainty in predictions plays a crucial role in Reinforcement Learning (RL). Many works incorporate uncertainty to guide exploration, directing it toward regions of high uncertainty (e.g., Lee et al. [2021], Liu et al. [2021], Ciosek et al. [2019], Osband et al. [2016]). Chua et al. [2018], Fu et al. [2022], and Janner et al. [2019] utilize ensembles of models to capture and represent uncertainty in learned environment dynamics, employing these models for planning purposes. In other cases, deep ensembles effectively mitigate overestimation bias in Q-value functions and enhance stability (Chen et al. [2021]).

Methods using ensembles have become popular for uncertainty modeling in deep neural networks. Ensembles combine several individual predictors. An ensemble’s predictive performance depends on individual performance, and the diversity of individual members plays an important role. Recent work, Abe et al. [2023], Abe et al. [2022a], points out how the diversity of the members gets reduced as the networks get larger. The effectiveness of uncertainty quantification using an ensemble of deep neural networks has been shown to reduce as the predictive ability of the ensemble members increases. This can be attributed to having large enough in-distribution data, big ensemble size, or over-parameterized networks. Having training objectives that train an ensemble to make diverse predictions may seem like a possible solution, but this can harm the predictive performance (Abe et al. [2023]). This has driven recent research to understand the cases under which ensembles are truly effective. A good single model can outweigh the benefits of using an ensemble for making out-of-distribution predictions (Abe et al. [2022b]). However, diversity is still important for predictions in a limited data regime and can not be easily mitigated by increasing the model size without overfitting.

Work in recent years has explored methods for Bayesian inference to obtain predictive ensembles and has demonstrated efficacy in uncertainty estimation (Neal [2012], Mackay [1992]). In Bayesian inference, one usually cares about the distribution of model parameters. Once this distribution is estimated, it can be used to make predictions by marginalizing. The way to approach this in a tractable manner is referred to as Bayesian Model Averaging. Such a class of methods has been shown to improve generalization, enhance uncertainty quantification, and improve model reliability in handling out-of-distribution data.

Traditional approaches to Bayesian inference depend on obtaining samples from Markov Chain Monte Carlo (MCMC) chains. These become computationally inefficient for bigger networks. Some approximate methods, such as stochastic gradient MCMC methods, manage to generate samples of the posterior distribution with the help of gradient information and use mini-batches of data. In comparison to these, Explicit variational methods are significantly better at inference time. This is because they directly optimize a tractable approximation of the true posterior, as opposed to depending on slower sampling methods like SG-MCMC. Implicit Variational methods, also known as Predictive Modeling, focus on directly estimating approximate posterior samples and have shown strong empirical performance. Posterior samples obtained using implicit methods constitute an ensemble of parameterized networks.

This paper considers a type of Implicit method: Particle optimization methods for approximate Bayesian Inference, which approximate the target distribution with an ensemble of networks acting as a set of particles. One common issue with these methods is that they often experience *mode collapse*. This occurs when the different members of the ensemble make similar predictions. Having functional diversity in posterior samples makes it easy to avoid averaging over similar functions, which leads to redundancy in the model average (D’Angelo and Fortuin [2021b], Wu et al. [2017], Pang et al. [2019]). This phenomenon of mode collapse is more evident when networks are over-parameterized (D’Angelo and Fortuin [2021b], Kirsch [2024]). It has been described as the problem of non-identifiability (Roeder et al. [2021]).

This work addresses the mode collapse issue and proposes a solution to ensure functional diversity using gradient information. It examines how functional diversity in particle optimization methods can be effectively controlled with kernel density estimation to approximate the target density. The paper introduces a simple method for training ensemble members for improved mode exploration and presents empirical results to validate the approach.

1.1 Contribution

In particular, the main contributions of this work are :

- A simple method to improve functional diversity by using kernel density as an approximation to the target distribution.
- Show how this results from the gradient flow of KL divergence between the target distribution and its approximation and Cross-Entropy of this approximation with kernel density.
- Empirically study the implications of the method and test its efficacy in improving planning using MPC for Model-Based RL.

2 Preliminaries

2.1 Bayesian Neural Networks (BNNs)

In a supervised learning setting, one has $D = \{X, Y\}$ where $X = \{x_i\}_{i=1}^N$ denoting the training inputs and $Y = \{y_i\}_{i=1}^N$ denote the corresponding outputs, with $x_i \in \mathcal{X}$ and $y_i \in \mathcal{Y}$, respectively. Let $f(x, \theta) : X \rightarrow \mathbb{R}^d$ denote a mapping function parameterized by a neural network, and one can define a likelihood function using this $p(y|f(x, \theta))$.

For example, a Gaussian for doing regression can be defined as :

$$p(y|f(x, \theta)) = \mathcal{N}(y|f(x; \theta), \sigma^2),$$

where σ^2 is the variance of observation noise.

For a classification problem with K classes, one could set $d = K$ and let

$$p(y|f(x, \theta)) = \text{Multinomial}(y|\text{softmax}(f(x; \theta))).$$

In Bayesian Neural Networks, the aim is to estimate the posterior distribution that captures all possible explanations for the given training data, defined as follows.

$$p(\theta|D) \propto \prod_{i=1}^N p(y_i|x_i, \theta)p(\theta)$$

$p(\theta)$ represents the prior distribution over the weight parameters θ . This helps capture a type of uncertainty called epistemic uncertainty. Epistemic uncertainty modeling especially shines when data is limited or additional data collection is difficult. Although many works use epistemic uncertainty methods when distributional shifts are present,

this could be potentially misleading. Ensembles are essential for improving predictive performance, uncertainty quantification, and robustness over a single model. However, their ability to quantify uncertainty and ensure robustness on out-of-distribution data correlates with their in-distribution performance. Work such as Malinin and Gales [2018] describes a non-parametric way to quantify uncertainty for such distribution shifts.

Most traditional ways to use neural network methods use a point estimate called a Maximum A Posteriori (MAP) estimate, which can be useful when sampling from a Bayesian Neural Network is challenging or when no model uncertainty needs to be captured.

Finally, to predict a test data point (x_{test}, y) , one can marginalize the entire posterior distribution rather than relying on a single parameter estimate.

$$p(y_{test}|x_{test}, D) = \int p(y_{test}|x_{test}, w)p(dw|D).$$

However, this integral is intractable for neural networks. It is typically approximated using Bayesian Model Averaging (BMA). Sampling-based methods for Bayesian Inference facilitate the acquisition of representative samples from such a posterior distribution to estimate this quantity. This becomes the reason why prediction accuracy in most approximate methods relies heavily on this Bayesian Model Averaging estimate.

$$p(y_{test}|x_{test}, D) \approx \frac{1}{M} \sum_{i=1}^M p(y_{test}|x_{test}, \theta_i)$$

2.2 Particle-optimization-based Variational Inference

This section describes how Implicit methods estimate the posterior as a stationary distribution by minimizing an energy functional. This can be modeled as a partial differential equation of the form :

$$\frac{\partial q_t}{\partial t} = -\nabla \cdot (v \cdot q_t),$$

where q_t is the approximate posterior at time t , and v is the gradient flow. This gradient flow depends on the choice of metric and energy functional. Samples obtained by simulating such a gradient flow constitute samples from this stationary distribution. In practice, numerical methods can be used for simulation. Particle-optimization based Variational Inference (POVI) methods approximate q_t with a set of particles $\{\theta^{(i)}\}_{i=1}^n$, i.e.,

$$q_t(\theta) \approx \frac{1}{n} \sum_{i=1}^n \delta(\theta - \theta_t^{(i)}),$$

and simulate the gradient flow with a discretized version of the ODE

$$\frac{d\theta_t^{(i)}}{dt} = -v(\theta_t^{(i)}).$$

The particles are updated using the following update in every iteration,

$$\theta_{t+1}^{(i)} \leftarrow \theta_t^{(i)} - \eta_t v(\theta_t^{(i)}),$$

where η_t is a step size.

In this way, implicit variational methods allow for the generation of samples without having to do probability evaluation for approximating the true posterior. Initial particle distribution plays a key role in the diversity of these samples. As the networks get larger, they become less and less sensitive to this initial distribution during training and converge to a single mode. This contrasts with Explicit variational methods, which approximate the posterior distribution by minimizing the KL divergence between a simpler, tractable distribution and the true posterior. Thus, the use of limited tractable distributions can hinder the accuracy of these methods.

Examples of POVI methods include Stein variational gradient descent (SVGD) Liu and Liu [2017], Liu et al. [2019], Chen et al. [2018], D’Angelo and Fortuin [2021b].

2.3 Gradient Flows

Different methods use different gradient flows. This section describes some of the most common choices of metric spaces and functionals for the gradient flow in POVI.

The p -Wasserstein distance for W_2 between ρ_0 and ρ_1 is defines a metric on $\mathcal{P}_2(\mathbb{R}^d)$ as

$$W_2^2(\rho_0, \rho_1) := \inf_{Y_0 \sim \rho_0; Y_1 \sim \rho_1} \mathbb{E}(\|Y_0 - Y_1\|^2) \quad (1)$$

$$= \inf_{\gamma \in \Pi(\rho_0, \rho_1)} \int_{\mathbb{R}^d \times \mathbb{R}^d} \|y_0 - y_1\|^2 d\gamma(y_0, y_1). \quad (2)$$

It can be understood as an optimal transport problem, where one wants to transform elements in the domain of ρ_0 to ρ_1 with a minimum cost.

Considering the optimization problem of a functional $F : \mathcal{P}_2(\mathcal{M}) \rightarrow \mathbb{R}$, the evolution in time of the measure ρ under the Wasserstein gradient flow is described by

$$\frac{\partial \rho(x)}{\partial t} = \nabla \cdot \left(\rho(x) \nabla \frac{\delta}{\delta \rho} F(\rho) \right). \quad (3)$$

as described in Jordan et al. [1998], Liu and Liu [2017] in detail where

$$\nabla \frac{\delta}{\delta \rho} F(\rho) =: \nabla_{\mathcal{W}_2} F(\rho, \pi)$$

is the Wasserstein gradient with a target measure, and the operator

$$\frac{\delta}{\delta \rho} : \mathcal{P}_2(\mathcal{M}) \rightarrow \mathbb{R}$$

represents the functional derivative.

Some examples of Particle-Optimization Sampling methods that use Wasserstein gradient flow are D'Angelo and Fortuin [2021b], which uses kernel density to approximate the target distribution. Chen et al. [2018] presents a novel particle-optimization framework grounded in Wasserstein gradient flows to unify two prominent scalable Bayesian sampling methods: stochastic gradient Markov chain Monte Carlo (SG-MCMC) and Stein variational gradient descent (SVGD).

D'Angelo and Fortuin [2021b] shows how SVGD can be reinterpreted as a gradient flow in the Wasserstein space under a particular Stein geometry induced on the manifold by the kernel and where \mathbb{K}_ρ is the metric. If $\mathbb{K}_\rho(\phi)(x)$ is a linear operator defined as $\mathbb{E}_{x' \sim \rho}[k(x, x')\phi(x')]$, the ODE describing the SVGD update becomes :

$$\frac{dx_i}{dt} = \mathbb{K}_\rho \nabla_{x'} (\log \pi(\mathbf{x}') - \log \rho(x'))$$

3 Deep Ensembles by ERGD

Empirical evidence and theoretical analysis Zhuo et al. [2018] have shown that particles in methods such as SVGD exhibit mode collapse. They converge to a limited number of local modes. Many works have proposed solutions to optimize for mode coverage by considering the impact of the interaction between the particles. This phenomenon is strongly related to the particles' initial distribution and becomes worse as the dimensionality increases. This section introduces a method to enhance mode coverage by mitigating the ensemble's dependence on the initial distribution while accounting for particle interactions within the ensemble.

The proposed method is called Entropy-Regularized Gradient Estimators. It uses an empirical measure of particles to approximate the target posterior. These set of particles are taken from an initial distribution and are evolved using the following update :

$$\frac{dx_i}{dt} = \frac{1}{n} \sum_{j=1}^n (k(\mathbf{x}_i, \mathbf{x}_j) \nabla_{\mathbf{x}_j} \log \pi(\mathbf{x}_j) - \beta \nabla_{\mathbf{x}_i} k(\mathbf{x}_i, \mathbf{x}_j)) \quad (4)$$

As in most similar works, a symmetric kernel models the interaction between the particles to train an ensemble. ERGD introduces a regularization constant that controls the effect of this interaction on functional diversity. The key idea behind this is that using kernel density as an approximation to the target density, the constant regularizes cross-entropy between the kernel density and this approximation. Intuitively, the evolution of the particles is influenced more by their interactions with each other.

$$\frac{dx}{dt} = - \int \left(k(\mathbf{x}, \mathbf{x}') \left[\nabla_{\mathbf{x}'} \frac{\delta}{\delta \rho} \left((-1 + \beta) H(\rho, \kappa) + D_{KL}(\rho, \pi) \right) \right] \rho(\mathbf{x}') \right) dx' \quad (5)$$

This update is similar to the SVGD update except for the regularization term. The evolution of the particles depends upon two types of updates. The first part on the right side considers the interaction between the particles as the attraction between them, and the second term is the repulsive term. Any symmetric kernel from the Stein Class can be used as an approximation to the target density.

The convergence guarantees of the method determine the choice for this regularization constant. As $\lim_{t \rightarrow \infty} \beta \rightarrow 1$, $\rho = \pi$ is a solution of the corresponding Liouville Equation (more details in Appendix A). A simple choice for β satisfying this is to use a linear schedule between positive value bigger than 1 to 1. This provides a method to guide particle evolution, placing much greater emphasis on the interactions between the particles in the initial distribution.

Using a symmetric kernel as an approximation to target probability density changes the gradient flow of KL divergence between two distributions under the metric induced by the Stein Operator to the gradient flow of KL divergence under the Wasserstein Metric (D'Angelo and Fortuin [2021b]). The following update gives the particle evolution method described in D'Angelo and Fortuin [2021b] :

$$\frac{dx_i}{dt} = \nabla_{\mathbf{x}_i} \log \pi(\mathbf{x}_i) - \beta \sum_{j=1}^k \nabla_{\mathbf{x}_i} k(\mathbf{x}_i, \mathbf{x}_j) \quad (6)$$

It can be understood as having the ensemble members grow without attraction, leading to a high probability density. In this case, the authors used β as $1 / \sum_{j=1}^k k(\mathbf{x}_i, \mathbf{x}_j)$. Such a β can be bad in practice (D'Angelo and Fortuin [2021b], D'Angelo and Fortuin [2021b]). Kirsch [2024] developed gradient estimators by inverting Stein's Identity. The work demonstrates that their method of selecting β outperforms the gradient estimator proposed in D'Angelo and Fortuin [2021b], as their estimator accounts for the effects of all interactions on a particle, including those not involving the particle itself. ERGD can direct particle evolution based on an initial distribution, but its performance depends on this initial distribution. In order to find a distribution that optimizes for mode coverage, ERGD is extended to s -ERGD as follows :

$$\frac{dx_i}{dt} = \nabla_{\mathbf{x}_i} \log \pi(\mathbf{x}_i) - \frac{\beta}{n} \sum_{j=1}^k \nabla_{\mathbf{x}_i} k(\mathbf{x}_i, \mathbf{x}_j) \quad (7)$$

s -ERGD update makes β a tunable parameter in the algorithm. Experiments comparing different updates use $\beta > 1$ for s -ERGD. Although this update is similar to Eq(6), it does not guarantee convergence.

4 Experiments

This section describes experiments to compare ERGD and s -ERGD with other POVI methods and Deep Ensembles.

4.1 Bivariate Gaussian Mixture

The first set of experiments tests how well different methods fit Gaussian mixture model. The centers for these Gaussians are at (213, 200), (180, 200), (200, 210), (200,190) with weights 0.6, 0.3, 0.05, 0.05. The experiments use 300 particles initialized at (180, 180).

It is important to note that s -ERGD may fail to converge in certain cases. Using ERGD with a linear schedule still fails to capture all modes of the distribution. D'Angelo and Fortuin [2021a] suggests that a linear schedule could result in slower training dynamics and proposed the use of a cyclic tanh schedule as an alternative. While ERGD with a tanh schedule can capture some of the modes, it does not necessarily guarantee complete mode discovery. On the other hand, s -ERGD is capable of exploring the distribution more effectively. Therefore, in the second-to-last figure of the final row, s -ERGD is employed to obtain an initial distribution, which is subsequently converges to the final solution using a linear schedule. This approach allows s -ERGD to serve as a way to have an initial distribution, while having the convergence properties associated with ERGD.

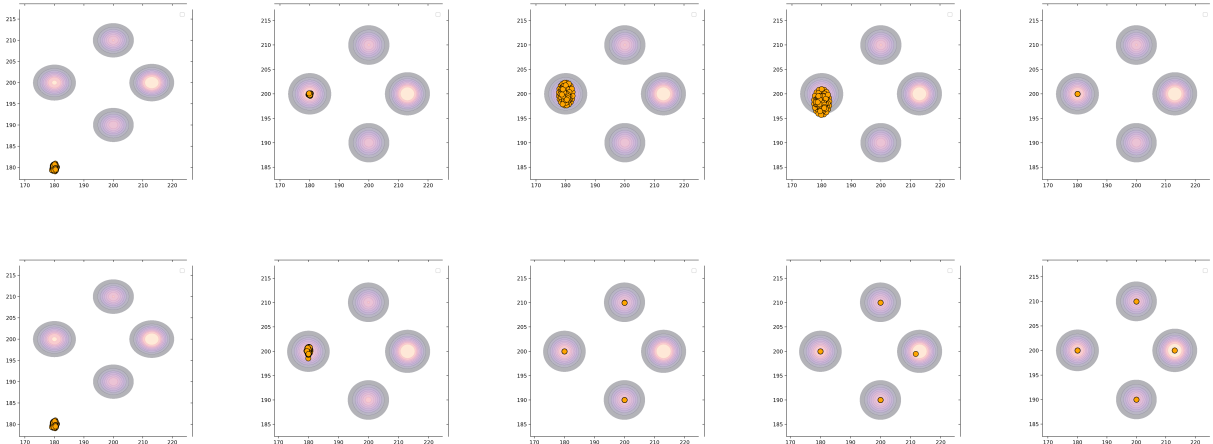


Figure 1: Starting from top row left - Initial Distribution, SVGD, kde-WGD, sse-WGD, SGD. Initial Distribution, ERGD with a linear and tanh schedule, ERGD with s -ERGD for an initial Distribution followed by a linear schedule and s -ERGD.

4.2 Classification Tasks

The classification experiments are conducted on the CIFAR-10 dataset and Fashion-MNIST dataset. The results report the performance of all the methods in terms of accuracy on the test data and negative-log-likelihood. The ratio between predictive entropy on OOD and test data points (H_o/H_t) and the model disagreement (MD) ratio tests the diversity of the ensemble generated by the different methods. The results are averaged over 5 random seeds. SVHN dataset is used as the OOD benchmark for CIFAR-10 and MNIST dataset as the OOD benchmark for Fashion-MNIST.

Different methods are compared for an ensemble size of 10 and 20 for the classification of CIFAR-10 and FMNIST, respectively. Classification on CIFAR-10 is done using ResNet 20 and Fashion-MNIST uses a neural network with 3 hidden layers and 128 hidden units. ERGD and s -ERGD are compared with SGD, kde -WGD using an update rule given by [6], sse -WGD as described in Kirsch [2024] and SVGD. ERGD uses a linear annealing schedule. For s -ERGD, experiments use a constant value of beta in order to compare with kde -WGD and sse -WGD.

ERGD performs better than SVGD and is comparative to kde -WGD and sse -WGD for both the datasets. Deep Ensembles perform comparative to kde -WGD on CIFAR-10 and have comparative performance to s -ERGD on FMNIST.

Method	Accuracy	NLL
Deep Ensembles	85.93 ± 2.55	0.29 ± 0.02
SVGD	85.35 ± 1.17	0.28 ± 0.03
kde WGD	85.625 ± 0.891	0.274 ± 0.02
sse WGD	85.979 ± 1.06	0.279 ± 0.02
ERGD	85.625 ± 3.68	0.28 ± 0.03
s ERGD	83.75 ± 2.61	0.32 ± 0.03

Method	H_o/H_t	MD_o/MD_t
Deep Ensembles	2.303 ± 0.12	1.878 ± 0.16
SVGD	2.211 ± 0.28	1.954 ± 0.25
kde WGD	2.319 ± 0.38	1.97 ± 0.31
sse WGD	2.152 ± 0.25	1.891 ± 0.26
ERGD	2.216 ± 0.3	1.927 ± 0.23
s ERGD	2.111 ± 0.192	1.74 ± 0.22

Table 1: *BNN Image Classification on CIFAR 10.*

Method	Accuracy	NLL
Deep Ensembles	89.296 \pm 2.13	0.179 \pm 0.02
SVGD	90.859 \pm 1.671	0.13 \pm 0.01
<i>kde</i> WGD	91.33 \pm 1.57	0.127 \pm 0.017
<i>sse</i> WGD	91.016 \pm 1.63	0.128 \pm 0.02
ERGD	91.016 \pm 1.56	0.127 \pm 0.02
<i>s</i> ERGD	89.531 \pm 1.596	0.182 \pm 0.02

Method	H_o/H_t	MD_o/MD_t
Deep Ensembles	4.382 \pm 0.57	5.983 \pm 0.637
SVGD	5.819 \pm 1.11	6.218 \pm 1.05
<i>kde</i> WGD	5.96 \pm 1.138	6.31 \pm 1.16
<i>sse</i> WGD	5.884 \pm 1.195	6.231 \pm 1.164
ERGD	5.67 \pm 0.921	6.12 \pm 0.86
<i>s</i> ERGD	4.331 \pm 0.53	5.984 \pm 0.631

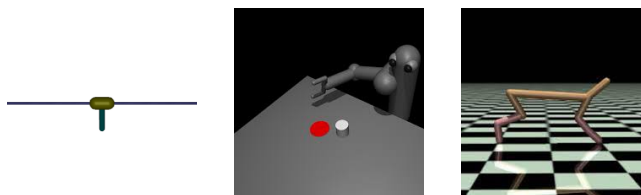
Table 2: *BNN Image Classification on FMNIST.*

Figure 2: Mujoco Environments [Todorov et al. [2012]]

4.3 Multi-Step Predictions for Model-Based RL

This section presents experiments for model-based RL to test how well an ensemble’s diverse predictions can be utilized to learn well when limited data is available. The section tests its efficacy in planning using uncertainty-aware model dynamics. The experiments use the algorithm probabilistic ensembles with trajectory sampling (PETS) proposed in Chua et al. [2018]. PETS selects actions using model-predictive control. It plans for short horizons and optimizes for this by using ensembles to make model predictions for different action sequences. It solves tasks such as continuous cartpole, half cheetah, pusher, and reacher in less than 100,000 environment interactions. It has been shown to perform more efficiently than SAC, PPO, or DDPG.

Experiments compare different ensembling methods with Deep Ensembles used in PETS. The ensembles are not trained from scratch at the start of every new episode. At the end of every episode, the converged target posterior informs training for the next episode. These experiments use an ensemble of 5 members and show results for all different optimization methods described above compared with SGD, which is used in PETS. Currently, this has been done for three environments: continuous cart pole, half-cheetah, and pusher. The planning horizon for both half-cheetah and pusher is 30, and that for the cart pole is 25. Experiments are average episode rewards over 400 episodes of length 1000 for Halfcheetah, 50 episodes of length 100 for Pusher and 50 episodes of length 200 for Cartpole. Results in Table 3 are mean over only 2 runs for Halcheetah and Pusher and 3 runs for Carpole.

5 Related Work

Deep Ensembles are an effective way of quantifying uncertainty while naively maintaining functional diversity with no strong guarantee (Wilson and Izmailov [2020] Izmailov et al. [2018]). This is theoretically motivated by using constant SGD as an approximate Bayesian posterior inference algorithm (Stephan et al. [2017]). Maddox et al. [2019] builds on the idea of Stochastic Weight Averaging. It estimates a Gaussian approximation using stochastic gradient descent (SGD) with a constant learning rate and averaging the weights throughout training. Wilson and Izmailov [2020] integrate this concept with an underlying ensemble structure based on multiple runs of SWAG. Finding parameter-efficient ensembles has been considered by Gal and Ghahramani [2016], Srivastava et al. [2014], and Maddox et al. [2019]. Maddox et al.

Method	Cartpole	Pusher	Halfcheetah
Deep Ensembles	195.74 ± 0.73	-68.99 ± 0.99	5393.68 ± 1441.12
SVGD	197.25 ± 2.11	-53.321 ± 1.28	3599.64 ± 292.95
<i>kde</i> WGD	196.94 ± 0.29	-45.38 ± 3.15	5178.73 ± 644.01
<i>sse</i> WGD	196.48 ± 1.04	-50.81 ± 2.3	4984.58 ± 807.59
ERGD	196.94 ± 0.45	-49.48 ± 0.58	6184.95 ± 908.18
sERGD	196.02 ± 0.56	-62.13 ± 9.415	4449.11 ± 441.31

Table 3: Average Episode Reward for Mujoco Environments.

[2019] tackles the issue of scalability and efficiency of Bayesian Neural Networks using rank-1 approximation to the weight matrices.

The significance of training ensembles to produce diverse predictions has long been a standard approach. However, recent studies have gone in depth in understanding the independent effect of using ensembles. Some works suggest that increasing diversity during training often leads to less effective ensembles. Abe et al. [2022a] views it from Jensen’s gap. Theisen et al. [2024] indicates that as long as the disagreement rate exceeds the average error rate, the ensemble continues to exhibit robust performance. Given extensive data, ensembling large networks does not prove more effective because it is not as sensitive to random initialization (Abe et al. [2023]). Ensembling smaller networks works better. Works such as Mania and Sra [2020], Abe et al. [2022b] show that an ensemble’s performance on out-of-distribution data depends on its performance on in-distribution data, and a larger single model can replicate the major benefits.

Many works have explored ways to give diverse predictions. Annealed Stein’s Variational Gradient Descent provides a way to avoid the mode collapse by using a cyclic annealing for SVGD (D’Angelo and Fortuin [2021a]). It is based on rescaling the target distribution by tempering the posterior. The annealing aims to provide a well-explored initialization, and a linear schedule from [0,1] does not work well because of slow dynamics. To better trade-off exploration and convergence, they use cyclic hyperbolic annealing. Experiments for ERGD and s-ERGD use a linear schedule for β between 1 and a positive constant, which works well for the entire training. Stein Variational Policy Gradient Descent has utilized a similar approach for regularizing the policy objective by tempering the target posterior.

In the context of POVI, making diverse predictions in weight-space does not mitigate the issue of non-identifiability in large networks, and function-space methods as described in D’Angelo and Fortuin [2021b] and Sun et al. [2019] perform better.

5.1 Conclusion

This paper provides a simple method for dealing with the issue of mode collapse in particle-based optimization methods. It highlights how having a symmetric kernel to model the interaction between the particles can be used to control the diversity in evolving particles. It proposes a way to train an ensemble by regularizing against this interaction. The work establishes the use of the method for classification tasks and shows how it can be helpful for efficient training for uncertainty-aware dynamics models. This demonstrates a way to reduce the dependence of the ensemble diversity on initial distribution while considering the particle interaction during training.

5.2 Acknowledgments

I would like to thank Amy Zhang for their guidance, insightful discussions and feedback that were instrumental in shaping the direction of this study. Suggestions they provided facilitated the development of the methodology and without their encouragement and advice, this work would not have been possible.

References

Taiga Abe, E Kelly Buchanan, Geoff Pleiss, and John Patrick Cunningham. The best deep ensembles sacrifice predictive diversity. In *I Can’t Believe It’s Not Better Workshop: Understanding Deep Learning Through Empirical Falsification*, 2022a.

- Taiga Abe, Estefany Kelly Buchanan, Geoff Pleiss, Richard Zemel, and John P Cunningham. Deep ensembles work, but are they necessary? *Advances in Neural Information Processing Systems*, 35:33646–33660, 2022b.
- Taiga Abe, E Kelly Buchanan, Geoff Pleiss, and John P Cunningham. Pathologies of predictive diversity in deep ensembles. *arXiv preprint arXiv:2302.00704*, 2023.
- Changyou Chen, Ruiyi Zhang, Wenlin Wang, Bai Li, and Liqun Chen. A unified particle-optimization framework for scalable bayesian sampling. *arXiv preprint arXiv:1805.11659*, 2018.
- Xinyue Chen, Che Wang, Zijian Zhou, and Keith Ross. Randomized ensembled double q-learning: Learning fast without a model. *arXiv preprint arXiv:2101.05982*, 2021.
- Kurtland Chua, Roberto Calandra, Rowan McAllister, and Sergey Levine. Deep reinforcement learning in a handful of trials using probabilistic dynamics models. *Advances in neural information processing systems*, 31, 2018.
- Kamil Ciosek, Quan Vuong, Robert Loftin, and Katja Hofmann. Better exploration with optimistic actor critic. *Advances in Neural Information Processing Systems*, 32, 2019.
- Francesco D’Angelo and Vincent Fortuin. Annealed stein variational gradient descent. *arXiv preprint arXiv:2101.09815*, 2021a.
- Francesco D’Angelo and Vincent Fortuin. Repulsive deep ensembles are bayesian. *Advances in Neural Information Processing Systems*, 34:3451–3465, 2021b.
- Haotian Fu, Shangqun Yu, Michael Littman, and George Konidaris. Model-based lifelong reinforcement learning with bayesian exploration. *Advances in Neural Information Processing Systems*, 35:32369–32382, 2022.
- Yarin Gal and Zoubin Ghahramani. Dropout as a bayesian approximation: Representing model uncertainty in deep learning. In *international conference on machine learning*, pages 1050–1059. PMLR, 2016.
- Pavel Izmailov, Dmitrii Podoprikin, Timur Garipov, Dmitry Vetrov, and Andrew Gordon Wilson. Averaging weights leads to wider optima and better generalization. *arXiv preprint arXiv:1803.05407*, 2018.
- Michael Janner, Justin Fu, Marvin Zhang, and Sergey Levine. When to trust your model: Model-based policy optimization. *Advances in neural information processing systems*, 32, 2019.
- Michael I. Jordan, Kevin P. Murphy, and Robert J. Adams. Introduction to variational methods for graphical models. *Machine Learning*, 37(2):183–233, 1998.
- Andreas Kirsch. (implicit) ensembles of ensembles: Epistemic uncertainty collapse in large models. *arXiv preprint arXiv:2409.02628*, 2024.
- Kimin Lee, Michael Laskin, Aravind Srinivas, and Pieter Abbeel. Sunrise: A simple unified framework for ensemble learning in deep reinforcement learning. In *International Conference on Machine Learning*, pages 6131–6141. PMLR, 2021.
- Chang Liu, Jingwei Zhuo, Pengyu Cheng, Ruiyi Zhang, and Jun Zhu. Understanding and accelerating particle-based variational inference. In *International Conference on Machine Learning*, pages 4082–4092. PMLR, 2019.
- Iou-Jen Liu, Unnat Jain, Raymond A Yeh, and Alexander Schwing. Cooperative exploration for multi-agent deep reinforcement learning. In *International conference on machine learning*, pages 6826–6836. PMLR, 2021.
- Jianqing Liu and Jun S. Liu. Stein variational gradient descent: A general purpose bayesian inference algorithm. *Journal of the American Statistical Association*, 112(518):897–908, 2017.
- David John Cameron Mackay. *Bayesian methods for adaptive models*. California Institute of Technology, 1992.
- Wesley J Maddox, Pavel Izmailov, Timur Garipov, Dmitry P Vetrov, and Andrew Gordon Wilson. A simple baseline for bayesian uncertainty in deep learning. *Advances in neural information processing systems*, 32, 2019.
- Andrey Malinin and Mark Gales. Predictive uncertainty estimation via prior networks. *Advances in neural information processing systems*, 31, 2018.
- Horia Mania and Suvrit Sra. Why do classifier accuracies show linear trends under distribution shift? *arXiv preprint arXiv:2012.15483*, 2020.
- Radford M Neal. *Bayesian learning for neural networks*, volume 118. Springer Science & Business Media, 2012.
- Ian Osband, Charles Blundell, Alexander Pritzel, and Benjamin Van Roy. Deep exploration via bootstrapped dqn. *Advances in neural information processing systems*, 29, 2016.
- Tianyu Pang, Kun Xu, Chao Du, Ning Chen, and Jun Zhu. Improving adversarial robustness via promoting ensemble diversity. In *International Conference on Machine Learning*, pages 4970–4979. PMLR, 2019.
- Geoffrey Roeder, Luke Metz, and Durk Kingma. On linear identifiability of learned representations. In *International Conference on Machine Learning*, pages 9030–9039. PMLR, 2021.

- Nitish Srivastava, Geoffrey Hinton, Alex Krizhevsky, Ilya Sutskever, and Ruslan Salakhutdinov. Dropout: a simple way to prevent neural networks from overfitting. *The journal of machine learning research*, 15(1):1929–1958, 2014.
- Mandt Stephan, Matthew D Hoffman, David M Blei, et al. Stochastic gradient descent as approximate bayesian inference. *Journal of Machine Learning Research*, 18(134):1–35, 2017.
- Shengyang Sun, Guodong Zhang, Jiabin Shi, and Roger Grosse. Functional variational bayesian neural networks. *arXiv preprint arXiv:1903.05779*, 2019.
- Ryan Theisen, Hyunsuk Kim, Yaoqing Yang, Liam Hodgkinson, and Michael W Mahoney. When are ensembles really effective? *Advances in Neural Information Processing Systems*, 36, 2024.
- Emanuel Todorov, Tom Erez, and Yuval Tassa. Mujoco: A physics engine for model-based control. In *2012 IEEE/RSJ International Conference on Intelligent Robots and Systems*, pages 5026–5033. IEEE, 2012. doi:10.1109/IROS.2012.6386109.
- Andrew G Wilson and Pavel Izmailov. Bayesian deep learning and a probabilistic perspective of generalization. *Advances in neural information processing systems*, 33:4697–4708, 2020.
- Jian Wu, Matthias Poloczek, Andrew G Wilson, and Peter Frazier. Bayesian optimization with gradients. *Advances in neural information processing systems*, 30, 2017.
- Jingwei Zhuo, Chang Liu, Jiabin Shi, Jun Zhu, Ning Chen, and Bo Zhang. Message passing stein variational gradient descent. In *International Conference on Machine Learning*, pages 6018–6027. PMLR, 2018.

A Appendix

A.1 The gradient flow of ERGD

In the following section, it can be shown that ERGD minimizes the KL Divergence between the target distribution, and its approximation and CrossEntropy between the approximation and the kernel. As described in D'Angelo and Fortuin [2021b], the particle evolution is described by the following equation.

$$\frac{dx_i}{dt} = \frac{1}{n} \sum_{j=1}^n (k(\mathbf{x}_i, \mathbf{x}_j) \nabla_{\mathbf{x}_j} \log \pi(\mathbf{x}_j) - \beta \nabla_{\mathbf{x}_i} k(\mathbf{x}_i, \mathbf{x}_j)) \quad (8)$$

$$\frac{dx}{dt} = \int (k(\mathbf{x}, \mathbf{x}') \nabla_{\mathbf{x}'} \log \pi(\mathbf{x}') + \nabla_{\mathbf{x}'} k(\mathbf{x}, \mathbf{x}')) \rho(x') dx' + \int (-\nabla_{\mathbf{x}'} k(\mathbf{x}, \mathbf{x}') - \beta \nabla_{\mathbf{x}} k(\mathbf{x}, \mathbf{x}')) \rho(x') dx' \quad (9)$$

Because of the symmetry of the kernel, the equation can be written as :

$$\frac{dx}{dt} = \int (k(\mathbf{x}, \mathbf{x}') \nabla_{\mathbf{x}'} \log \pi(\mathbf{x}') + \nabla_{\mathbf{x}'} k(\mathbf{x}, \mathbf{x}')) \rho(x') dx' + \int (-\nabla_{\mathbf{x}'} k(\mathbf{x}, \mathbf{x}') + \beta \nabla_{\mathbf{x}} k(\mathbf{x}, \mathbf{x}')) \rho(x') dx' \quad (10)$$

$$\frac{dx}{dt} = \int (k(\mathbf{x}, \mathbf{x}') \nabla_{\mathbf{x}'} \log \pi(\mathbf{x}') + \nabla_{\mathbf{x}'} k(\mathbf{x}, \mathbf{x}')) \rho(x') dx' + \int ((-1 + \beta) \nabla_{\mathbf{x}'} k(\mathbf{x}, \mathbf{x}')) \rho(x') dx' \quad (11)$$

$$\frac{dx}{dt} = \int \left(k(\mathbf{x}, \mathbf{x}') \nabla_{\mathbf{x}'} \log \pi(\mathbf{x}') + \nabla_{\mathbf{x}'} k(\mathbf{x}, \mathbf{x}') \rho(x') dx' + \int (-1 + \beta) \nabla_{\mathbf{x}'} \log k(\mathbf{x}, \mathbf{x}') \right) \rho(x') dx' \quad (12)$$

$$\begin{aligned} \frac{dx}{dt} = \int & k(\mathbf{x}, \mathbf{x}') \nabla_{\mathbf{x}'} \log \pi(\mathbf{x}') \rho(x') dx' + \nabla_{\mathbf{x}'} k(\mathbf{x}, \mathbf{x}') \rho(x') dx' - k(\mathbf{x}, \mathbf{x}') \rho(x') dx' + \\ & \int ((-1 + \beta) \nabla_{\mathbf{x}'} \log k(\mathbf{x}, \mathbf{x}')) \rho(x') dx' \end{aligned} \quad (13)$$

$$\begin{aligned} \frac{dx}{dt} = \int & k(\mathbf{x}, \mathbf{x}') \nabla_{\mathbf{x}'} \log \pi(\mathbf{x}') \rho(x') dx' - \int k(\mathbf{x}, \mathbf{x}') \nabla_{\mathbf{x}'} \rho(x') dx' + \\ & \int ((-1 + \beta) \nabla_{\mathbf{x}'} \log k(\mathbf{x}, \mathbf{x}')) \rho(x') dx' \end{aligned} \quad (14)$$

$$\begin{aligned} \frac{dx}{dt} = \int & k(\mathbf{x}, \mathbf{x}') \nabla_{\mathbf{x}'} \log \pi(\mathbf{x}') \rho(x') dx' - \int k(\mathbf{x}, \mathbf{x}') \nabla_{\mathbf{x}'} \log \rho(x') \rho(x') dx' + \\ & \int ((-1 + \beta) \nabla_{\mathbf{x}'} \log k(\mathbf{x}, \mathbf{x}')) \rho(x') dx' \end{aligned} \quad (15)$$

$$\begin{aligned} \frac{dx}{dt} = \int & k(\mathbf{x}, \mathbf{x}') (\nabla_{\mathbf{x}'} \log \pi(\mathbf{x}') - \nabla_{\mathbf{x}'} \log \rho(x')) \rho(x') dx' + \\ & \int ((-1 + \beta) \nabla_{\mathbf{x}'} \log k(\mathbf{x}, \mathbf{x}')) \rho(x') dx' \end{aligned} \quad (16)$$

$$\frac{dx}{dt} = - \int \left(k(\mathbf{x}, \mathbf{x}') \left[\nabla_{\mathbf{x}'} ((-1 + \beta) \frac{\delta}{\delta \rho} H(\rho, \kappa) + \nabla_{\mathbf{x}'} \frac{\delta}{\delta \rho} D_{KL}(\rho, \pi)) \right] \rho(x') dx' \right) \quad (17)$$

$$\frac{dx}{dt} = - \int \left(k(\mathbf{x}, \mathbf{x}') \left[\nabla_{\mathbf{x}'} \frac{\delta}{\delta \rho} ((-1 + \beta) H(\rho, \kappa) + D_{KL}(\rho, \pi)) \right] \rho(x') dx' \right) \quad (18)$$

B Experimental Details

B.1 Classification Tasks

For the CIFAR-10 classification task, ResNet-20 was trained over 50,000 epochs using a learning rate of 0.00025 across all methods, with 10 particles. Similarly, for FMNIST, ResNet-8 was trained for 50,000 epochs with a learning rate of 0.001 and an ensemble size of 10. A prior variance of 0.1 was used.

Table 4: Hyperparameters for CIFAR-10 Classification

Parameter	Value	Description
Ensemble Size	10	Number of Networks in the Ensemble
Learning Rate	0.00025	Controls the step size during optimization
Batch Size	128	Number of samples per batch
beta	1.6, 1.1	Entropy parameter for ERGD, sERGD
Epochs	50,000	Number of training iterations
Prior	Normal (0,0.1)	Prior for Network Parameters
Model Architecture	ResNet-20	Type of Model used
Random Seeds	77, 89, 65, 42, 23	Random Seeds for experiments

Table 5: Hyperparameters for FMNIST Classification

Parameter	Value	Description
Ensemble Size	20	Number of Networks in the Ensemble
Learning Rate	0.001	Controls the step size during optimization
Batch Size	256	Number of samples per batch
beta	1.6, 1.1	Entropy parameter for ERGD, sERGD
Epochs	50,000	Number of training iterations
Prior	Normal (0,0.1)	Prior for Network Parameters
Model Architecture	3 Layers, 128 units	Type of Model used
Random Seeds	77, 89, 65, 42, 23	Random Seeds for experiments

B.2 Model-Based RL

Table 6: Hyperparameters for HalfCheetah

Parameter	Value	Description
Ensemble Size	5	Number of Networks in the Ensemble
Number of Trials	400	Number of Episodes
Trial Length	1000	Length of each trial
Seed	98,78,42	Random seed value for experiments
Training Hidden Layers	3	Number of hidden layers in model
Training Hidden Size	256	Number of neurons in each hidden layer
Training Batch Size	256	Number of samples per batch
Training Beta	1.6	Beta parameter for training
Training Num Particles	20	Number of particles for training
Training Epochs	100	Number of training epochs
Training Learning Rate	0.001	Learning rate for training
Optimizer Iterations	5	Number of iterations for optimizer
Optimizer Alpha	0.1	Alpha parameter for optimizer
Optimizer Population Size	800	Population size for optimizer
Optimizer Planning Horizon	30	Planning horizon for optimizer

Table 7: Hyperparameters for Pusher

Parameter	Value	Description
Ensemble Size	5	Number of Networks in the Ensemble
Number of Trials	50	Number of Episodes
Trial Length	100	Length of each trial
Seed	98,78,42	Random seed value for experiments
Training Hidden Layers	3	Number of hidden layers in model
Training Hidden Size	500	Number of neurons in each hidden layer
Training Batch Size	32	Number of samples per batch
Training Beta	1.6	Beta parameter for training
Training Num Particles	20	Number of particles for training
Training Epochs	200	Number of training epochs
Training Learning Rate	0.001	Learning rate for training
Optimizer Iterations	5	Number of iterations for optimizer
Optimizer Alpha	0.1	Alpha parameter for optimizer
Optimizer Planning Horizon	25	Planning horizon for optimizer

Table 8: Hyperparameters for Cartpole

Parameter	Value	Description
Ensemble Size	5	Number of Networks in the Ensemble
Number of Trials	50	Number of Episodes
Trial Length	200	Length of each trial
Seed	98,78,42	Random seed value for experiments
Training Hidden Layers	3	Number of hidden layers in model
Training Hidden Size	256	Number of neurons in each hidden layer
Training Batch Size	256	Number of samples per batch
Training Beta	1.6	Beta parameter for training
Training Num Particles	20	Number of particles for training
Training Epochs	200	Number of training epochs
Training Learning Rate	0.001	Learning rate for training
Optimizer Iterations	5	Number of iterations for optimizer
Optimizer Alpha	0.1	Alpha parameter for optimizer
Optimizer Planning Horizon	25	Planning horizon for optimizer